PREPARED FOR THE U.S. DEPARTMENT OF ENERGY,
UNDER CONTRACT DE-AC02-76CH03073

PPPL-3809
UC-70

PPPL-3809

Near-earth Thin Current Sheets and Birkeland Currents during Substorm Growth Phase

by

Sorin Zaharia and C.Z. Cheng

April 2003

PRINCETON PLASMA PHYSICS LABORATORY

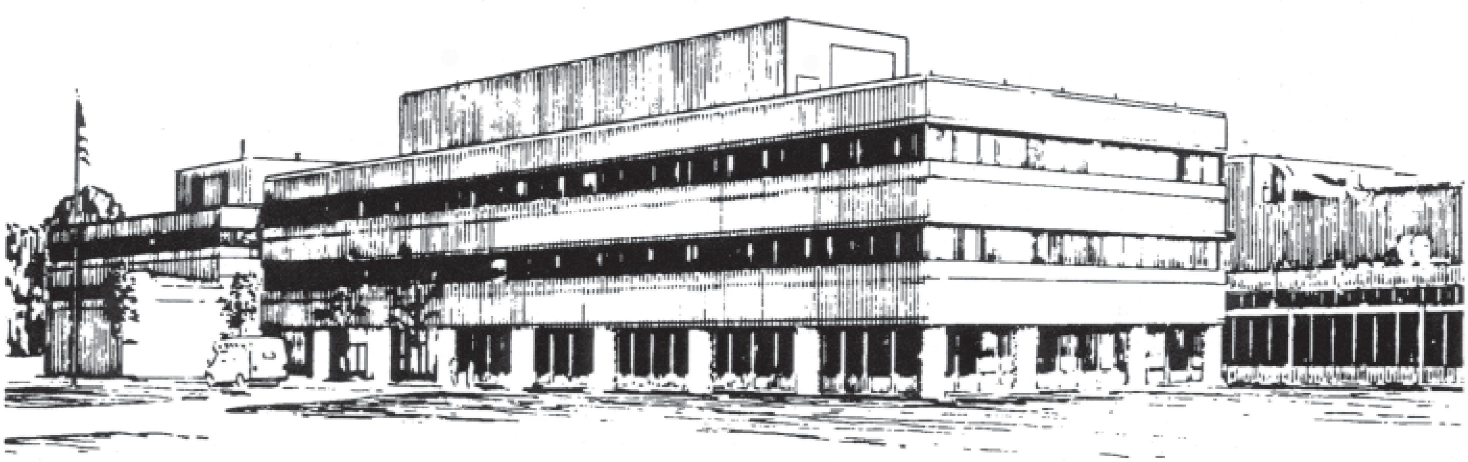

PRINCETON PLASMA PHYSICS LABORATORY
PRINCETON UNIVERSITY, PRINCETON, NEW JERSEY

PPPL Reports Disclaimer

Availability

This report is posted on the U.S. Department of Energy's Princeton Plasma Physics Laboratory Publications and Reports web site in Fiscal Year 2003. The home page for PPPL Reports and Publications is: http://www.pppl.gov/pub_report/

DOE and DOE Contractors can obtain copies of this report from:

U.S. Department of Energy
Office of Scientific and Technical Information
DOE Technical Information Services (DTIS)
P.O. Box 62
Oak Ridge, TN 37831

Telephone: (865) 576-8401
Fax: (865) 576-5728
Email: reports@adonis.osti.gov

This report is available to the general public from:

National Technical Information Service
U.S. Department of Commerce
5285 Port Royal Road
Springfield, VA 22161

Telephone: 1-800-553-6847 or
(703) 605-6000
Fax: (703) 321-8547
Internet: http://www.ntis.gov/ordering.htm

Submitted to *Geophysical Research Letters,* 2003

Near-Earth thin current sheets and Birkeland currents during substorm growth phase

Sorin Zaharia and C. Z. Cheng

Plasma Physics Laboratory, Princeton University, Princeton, NJ 08543

Abstract. Two important phenomena observed during the magnetospheric substorm growth phase are modeled: the formation of a near-Earth ($|X| \sim 9\,R_E$) thin cross-tail current sheet, as well as the equatorward shift of the ionospheric Birkeland currents. Our study is performed by solving the 3-D force-balance equation with realistic boundary conditions and pressure distributions. The results show a cross-tail current sheet with large current ($J_\phi \sim 10\,\mathrm{nA/m^2}$) and very high plasma β ($\beta \sim 40$) between 7 and $10\,R_E$. The obtained region-1 and region-2 Birkeland currents, formed on closed field lines due to pressure gradients, move equatorward and become more intense ($J_{\|\max} \sim 3\,\mu\mathrm{A/m^2}$) compared to quiet times. Both results are in agreement with substorm growth phase observations. Our results also predict that the cross-tail current sheet maps into the ionosphere in the transition region between the region-1 and region-2 currents.

1. Introduction

Two important phenomena are associated with the substorm growth phase. One is the appearance of a thin cross-tail current sheet in the near-Earth (7 – $10\,R_E$) plasma sheet [e.g., *Sergeev et al.*, 1990]. The other consists in an intensity increase and an equatorward shift of the region-1 and region-2 ionospheric field-aligned (Birkeland) currents (with a similar shift being observed in the auroral arc structures [e.g., *Samson et al.*, 1992]). Using our 3-D quasi-equilibrium model [*Cheng*, 1995; *Zaharia et al.*, 2003] we investigate here these 2 effects, i.e. the formation of the cross-tail current sheet and the Birkeland current configuration, as well as their relationship during the substorm growth phase.

There is a consensus in the space physics community that the inner and middle magnetosphere on closed field lines is a "slow-flow" region [*Wolf*, 1983] at most times, including during the growth phase. Thus the inertial terms can be neglected in the plasma equation of motion and the magnetospheric evolution can be depicted as a temporal series of "snapshots", each of them a "quasi-static equilibrium" state in which force balance is maintained between the magnetic (Lorentz) force and the plasma pressure gradient force. Within the "slow flow" approximation there have been several theoretical efforts trying to explain thin current sheet formation. Most approaches [e.g., *Wiegelmann and Schindler*, 1995; *Birn and Schindler*, 2002] investigate the currents at $X < -20\,R_E$ (from here on X, Y and Z are the usual GSM coordinates), where the so-called tail approximation [*Birn et al.*, 1975] is valid, and the problem is sometimes even analytically tractable. Only a few studies [e.g., *Becker et al.*, 2001] look at the current sheets closer to Earth, where the tail approximation becomes inaccurate, and these studies assume 2-D axisymmetry, missing the formation of the field-aligned currents (a 3-D effect, as explained by *Cheng* [1995]). Most studies consider the magnetospheric evolution during the growth phase to be dictated by "adiabatic convection" [e.g., *Wolf*, 1983] whereby the entropy, related to the quantity $S = PV^\gamma$, is conserved (P is the pressure, V the magnetic flux tube volume per unit flux, $V = \int ds/B$, with the integral performed along a magnetic field line; $\gamma = 5/3$). With entropy conservation constraints a very thin current sheet can form for example due to deformations of the magnetopause boundary [*Birn and Schindler*, 2002].

In the inner tail ($|X| < 15\,R_E$) there are observational indications however [e.g., *Borovsky et al.*, 1998] that the entropy conservation is violated. Without entropy conservation, a process called entropy anti-diffusion has been proposed [*Lee et al.*, 1998] to explain thin current sheet formation. The magnetospheric evolution in the model of *Lee et al.* [1998] is however characterized by significant flows, a result not supported by observations during growth phase .

In this letter we discuss 3-D force-balanced magnetospheric configurations, focusing on the formation during the substorm growth phase of a thin current sheet in the near-Earth plasma sheet and on the changes in Birkeland currents compared to a quiet time state. Our configurations are obtained by solving numerically the 3-D force-balance equation $\mathbf{J}\times\mathbf{B} = \boldsymbol{\nabla}P$ in a flux coordinate system [*Cheng*, 1995; *Zaharia et al.*, 2003], subject to realistic flux boundary conditions and pressure distributions. The cause of the current sheet formation is the large value of $|\partial P/\partial\psi|$ caused by plasma and flux transport during the growth phase. The Birkeland currents, formed on closed field lines due to pressure gradients, move equatorward and become more intense ($J_{\parallel\,\max} \sim 3\,\mu\mathrm{A/m^2}$) compared to quiet times. The cross-tail current sheet region maps into the ionosphere in the transition region between the region-1 and region-2 currents.

2. Modeling approach

We work in a geomagnetic flux coordinate system $\{\psi, \alpha, \chi\}$, in which two of the coordinates, α and ψ, are Euler potentials for the magnetic field: $\mathbf{B} = \boldsymbol{\nabla}\psi \times \boldsymbol{\nabla}\alpha$. We choose ψ to label the magnetic flux and α an azimuthal angle-like function. The third coordinate, χ, is a function of the distance along the field line. The computation of equilibria in the $\{\psi, \alpha, \chi\}$ system, described in detail elsewhere [*Cheng*, 1995; *Zaharia et al.*, 2003], consists in solving the 3-D equation $\mathbf{J}\times\mathbf{B} = \boldsymbol{\nabla}P$ iteratively, subject to input pressure distribution and boundary conditions. The boundary ψ surfaces delimiting the computational domain have specified shapes, usually obtained [*Zaharia et al.*, 2003] from empirical models such as T96 [*Tsyganenko and Stern*, 1996]. We only briefly describe here the changes implemented in our method for a more accurate computation of configurations with strong current sheets. The first change was using as "planet boundary" a sphere of radius $2\,R_E$ instead of the Earth's surface. While the code can perfectly handle a computation from $1\,R_E$, this was done in order to save grid points for the important plasma sheet region. The second change was relaxing the "equal arc length" choice [*Cheng*, 1995] for χ, instead concentrating the grid points near the equatorial plane. The grid points are also non-uniformly distributed in azimuth [*Zaharia et al.*, 2003], with a concentration near the midnight meridian. The number of grid points used is $N_\psi \times N_\alpha \times N_\chi = 75^3$, leading to a spatial resolution near the equatorial plane at $R \sim 8\,R_E$ and midnight of about $\Delta X = 0.25\,R_E$, $\Delta Y = 0.25\,R_E$ and $\Delta Z = 0.05\,R_E$.

3. Results: quiet time vs. substorm growth phase

While our emphasis is on the substorm growth phase, we will discuss first a 3-D force-balanced quiet-time configuration in order to facilitate a discussion of differences between the two. For the quiet-time case we use inner and outer boundary shapes for ψ obtained by field-line tracing using the T96 model, with parameters $DST = -5\,\mathrm{nT}$, $P_{\mathrm{SW}} = 2.1\,\mathrm{nPa}$, $B_{\mathrm{yIMF}} = 0$ and $B_{\mathrm{zIMF}} = 1\,\mathrm{nT}$, representing average quiet-time parameters as obtained from the OMNI solar wind database. For the pressure P we choose the following form in the equatorial plane:

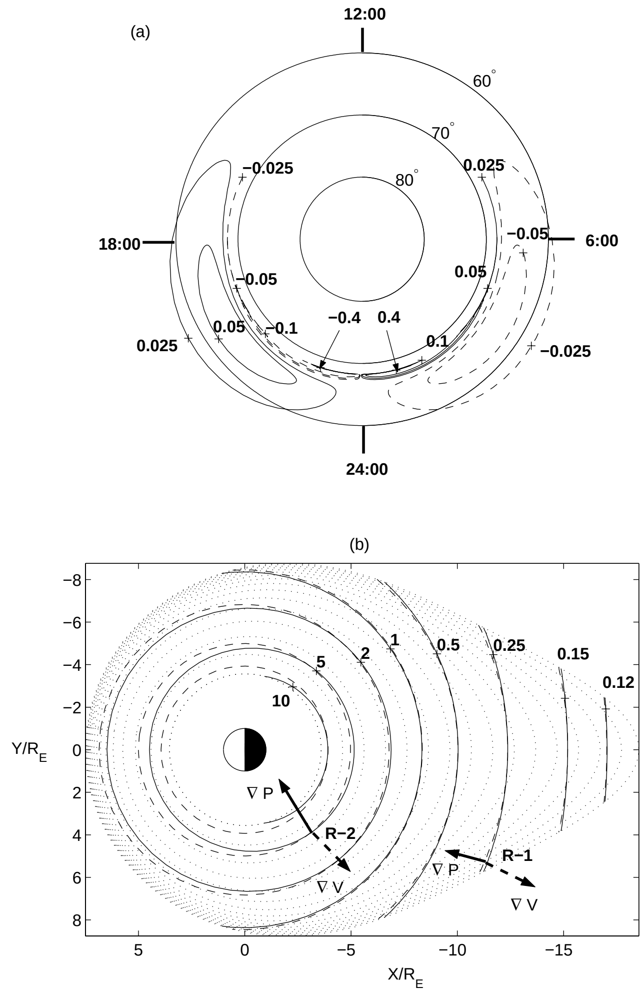

Figure 1. For the quiet-time state: (a) Contours of constant ionospheric $J_\parallel$ (μA); solid (dashed) lines represent currents into (out of) the ionosphere; (b) Equatorial plane contours of P(nPa) (solid) and V (dashed); also shown are $\boldsymbol{\nabla}P$ and $\boldsymbol{\nabla}V$ at two points mapping into regions of opposite $J_\parallel$ in the ionosphere; the dotted lines show const. ψ contours.

$$P(R,\phi,Z=0) = 89e^{-0.59R}\left[A + Be^{-\left(\frac{\phi-\pi}{\Delta\phi}\right)^2}\right] + 8.9R^{-1.53}\left[C + De^{-\left(\frac{\phi-\pi}{\Delta\phi}\right)^2}\right] \quad (1)$$

where R, ϕ, Z define the usual cylindrical coordinate system with Earth as origin and $\phi = \pi$ at midnight, while A, B, C, D and $\Delta\phi$ are constants. We choose $A = B = 0.5$,

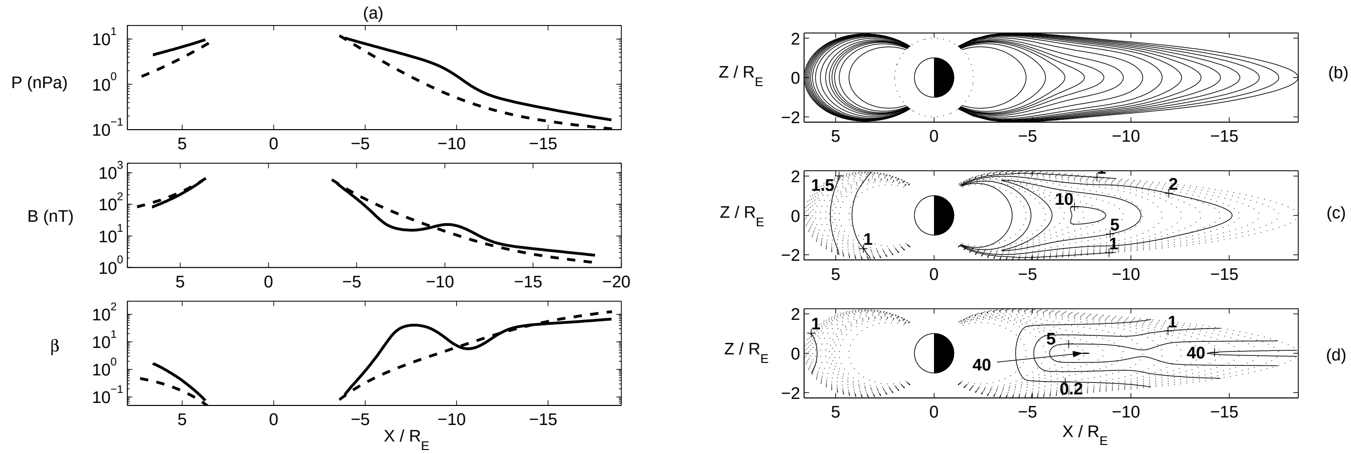

Figure 2. (a) Profiles of P, B and β along the Sun-Earth axis for the growth phase (solid) and quiet-time (dashed); For the growth phase, plots in the noon-midnight meridian plane of : (b) Magnetic field lines; (c) Constant J_ϕ (solid) and ψ (dotted) contours; (d) Constant β (solid) and ψ (dotted) contours.

$C = 2$, $D = -1$ and $\Delta\phi = 0.5\pi$, such that for $\phi = \pi$ Eq. (1) recovers the Spence-Kivelson empirical formula [*Spence and Kivelson*, 1993], which is based on observations at midnight. At the same time, since the first term on the RHS of Eq. (1) dominates close to Earth ($R < 10\,R_E$), while the second term farther in the tail, Eq. (1) also simulates for a given R an azimuthal maximum in P at midnight close to Earth, and an azimuthal minimum farther in the tail. This qualitative local-time dependence, seen in the equatorial P contours in Fig. 1(b), is justified by observations showing a maximum in P at midnight close to Earth [*De Michelis et al.*, 1999, e.g.,], but a slight minimum at midnight for $R > 10\,R_E$ (see Fig. 11 of [*Tsyganenko and Mukai*, 2003]).

We will only briefly summarize the physical parameters of the computed quiet-time state. The cross-tail current ($J_\phi = \mathbf{J}\cdot\boldsymbol{\nabla}\phi/|\boldsymbol{\nabla}\phi|$) has a maximum $J_\phi \approx 2.4\,\mathrm{nA/m^2}$. Dashed lines in Fig. 2(a) show the profiles along the Sun-Earth axis of P, B and plasma β for this case, while the Birkeland currents are shown in Fig. 1(a). The region-2 currents span a broad area, but are very weak ($J_{\|2\max} = 0.07\,\mu\mathrm{A/m^2}$) — consistent with observations [*Iijima and Potemra*, 1976] showing their virtual disappearance during quiet times. On the other hand, a more narrow region-1 current pattern exists at higher latitudes ($\sim 68^\circ$), with maximum densities ($\approx 0.5\,\mu\mathrm{A/m^2}$) at 11:00 and 2:00 local times, again agreeing very well with quiet-time observations [*Iijima and Potemra*, 1976]. The region-1 and region-2 current formation mechanism is easily understood from Vasyliunas relation [*Vasyliunas*, 1970], in the form

$$\frac{J_\|}{B}\Big|_{iono} = \frac{\mathbf{B}_{eq}}{B_{eq}^2}\cdot(\boldsymbol{\nabla}V \times \boldsymbol{\nabla}P_{eq}) \qquad (2)$$

The quantity $\mathbf{B}_{eq}\cdot(\boldsymbol{\nabla}P_{eq}\times\boldsymbol{\nabla}V)$ has opposite signs for region-1 vs. region-2 current formation, as seen in Fig. 1(b), which shows $\boldsymbol{\nabla}P$ and $\boldsymbol{\nabla}V$ at two equatorial plane locations that map into the ionosphere in regions of opposite $\mathbf{J}_\|$.

For modeling a substorm growth phase, the ψ boundary shapes are obtained again from T96, this time with $P_{SW} = 5\,\mathrm{nPa}$, $B_{\mathrm{ZIMF}} = -5\,\mathrm{nT}$, $B_{\mathrm{YIMF}} = 0.5\,\mathrm{nT}$ and $DST = -50\,\mathrm{nT}$, typical for disturbed times. There are only scarce plasma pressure observations during the growth phase. While P generally increases with activity throughout the plasma sheet [e.g., *Tsyganenko and Mukai*, 2003], observations [e.g. *Spence et al.*, 1989] as well as convection simulations [*Wang et al.*, 2003] show that the pressure enhancement is larger at smaller radial distances. Another property, both observed [*Wing and Newell*, 1998; *Tsyganenko and Mukai*, 2003] and apparent in simulations [*Wang et al.*, 2003, e.g.,], is the Earthward expansion of regions with azimuthal minimum P at midnight (for fixed R). We thus choose the P distribution in the equatorial plane as

$$P(R,\phi,Z=0) = 12.5e^{-0.25R}\cdot\left[A + B\tanh\left(\frac{x_1 - R}{\Delta R}\right)\right.$$
$$\left. e^{-\left(\frac{\phi-\pi}{\Delta\phi}\right)^2}\right] + 8.9R^{-1.53}\left[C + De^{-\left(\frac{\phi-\pi}{\Delta\phi}\right)^2}\right] \qquad (3)$$

We choose $A = 1.25$, $B = 0.75$, $C = 3$, $D = -2$, $\Delta\phi = 0.3\pi$, $x_1 = 10$ and $\Delta R = 1.25$ in Eq. (3). The resulting P profile along the Sun-Earth axis, shown by solid lines in Fig. 2(a), is about twice the quiet-time value tailward of $10\,R_E$, and even more enhanced at the inner edge of the plasma sheet. The equatorial P contours, shown in Fig. 3(b), show the Earthward expansion of regions with P minimum (for a given R) at midnight, and at the same time the more pronounced azimuthal minima in P as compared to the quiet-time case.

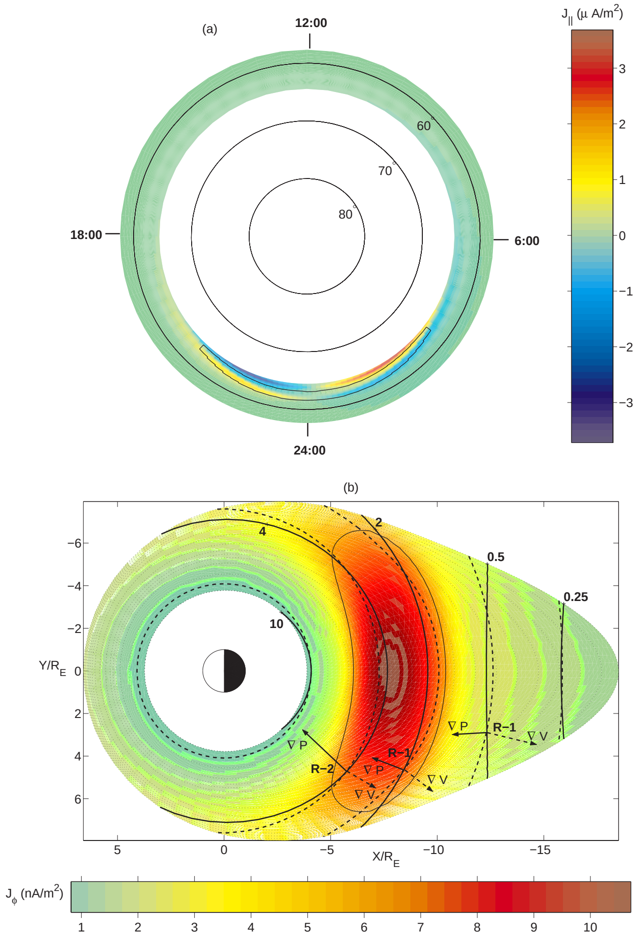

Figure 3. For the growth phase: (a) Ionospheric $J_{\|}$; (b) Equatorial plane P(nPa) contours (thick solid lines), V (dashed) and ψ (dotted), over a color plot of J_ϕ; the thin solid contour shows the region inside which $J_\phi > 0.5\, J_{\phi\max}$; also shown are $\mathbf{\nabla} P$ and $\mathbf{\nabla} V$ at three locations.

Figure 2 shows several quantities in the the obtained force-balanced state. The solid lines in Fig. 2(a) show profiles of P, B and β along the Sun-Earth axis. We notice the appearance of a local magnetic well, with $B_{\min} \approx 15\,\text{nT}$, between $X = -7\,R_E$ and $X = -9\,R_E$. In the magnetic well, plasma β peaks at $\beta \approx 45$ near $X = -8\,R_E$. The magnetic field is extremely tail-like in the near-Earth plasma sheet, as seen in Fig. 2(b). The tail-like field suggests a thin current sheet, which can indeed be seen in Fig. 2(c), which shows noon-midnight meridian plane contours of J_ϕ. The maximum current density is $J_{\phi\max} \approx 11\,\text{nA/m}^2$, and the sheet has a minimum half-width of $0.6\,R_E$ at $X = -9\,R_E$. Finally, from Fig. 2 (d) one notices that plasma β is very large in the vicinity of the equatorial plane.

The Birkeland currents in this state are shown in Fig. 3(a). Both the region-1 and region-2 currents have moved to lower latitudes compared to the quiet-time case shown in Fig. 1(a), and are much more intense (with the intense $J_{\|}$ regions quite peaked in latitudinal extent). The region-2 current has a maximum density of $1.2\,\mu\text{A/m}^2$ at 22:00 and 2:00 local times, and stretches between 60° and 62° in latitude. The region-1 current is found between 62° and 65° and has a maximum of $3.5\,\mu\text{A/m}^2$ closer to midnight (22:30 and 1:30 local times). Again, the different signs of $\mathbf{B}\cdot(\mathbf{\nabla} P\times\mathbf{\nabla} V)$ in the region-2 and region-1 current regions, respectively, are readily seen in Fig. 3(b), which shows the orientation of the vectors $\mathbf{\nabla} P$ and $\mathbf{\nabla} V$ over a color plot of J_ϕ in the equatorial plane. From Fig. 3 one observes that the cross-tail current sheet maps into the ionosphere into the transition area between region-1 and region-2 currents.

4. Discussion and Summary

We have modeled a quasi-static equilibrium magnetospheric state during the substorm growth phase, by solving the 3-D force-balance equation with realistic pressure and flux boundaries. The obtained configuration includes a thin current sheet with $J_\phi \sim 10\,\text{nA/m}^2$ in the near-Earth plasma sheet between $X = -7\,R_E$ and $X = -9\,R_E$. The configuration is also characterized by the region-1 and region-2 Birkeland currents moving toward lower latitudes (60° – 65°), and being more intense (region-1 $J_{\|1\,\max} \sim 3\,\mu\text{A/m}^2$) compared to quiet times. The cross-tail current sheet region maps into the ionosphere in the transition area between the region-1 and region-2 currents.

The near-Earth cross-tail current sheet has a half-thickness $\sim 0.6\,R_E$, in good agreement with observations [*Sanny et al.*, 1994] showing the current sheet being wider than $1\,R_E$ throughout the growth phase. This result differs from the popular belief that the sheet thickness is on the order of an ion gyro-radius ($\rho_i \leq 1000\,\text{km}$). It is unlikely that such currents can be found in a force-balanced configuration in the transition region between the dipole-like and tail-like magnetic field. Among the reasons for this, we note that direct evidence of extremely thin current sheets is scarce — most observations measure the **B**-field and try to fit it with an unrealistic very thin Harris current sheet, without discussing whether a thicker sheet might suffice. Secondly, observations in the near-Earth plasma sheet at $X \approx -8\,R_E$ by AMPTE/CCE [*Lui et al.*, 1992] show that the angle between the B_z and B_x components of **B** is never less than 40° at any time during the substorm growth phase, therefore precluding the existence of a sheet of width $\sim \rho_i$. Finally, we note that the current sheet does not need to become thinner than $\sim 0.5\,R_E$ in order to lead to substorm onset; indeed, in our current sheet region plasma β (~ 45) is already sufficiently large for a kinetic ballooning instability [*Cheng and Lui*, 1998] to be excited and lead to onset.

Based on our study, the scenario for current sheet formation near Earth ($|X| < 10\,R_E$) is the following: during the growth phase, the larger solar wind P_{SW} and increased flux merging at the magnetopause leads to enhanced tail stretching. At the same time, plasma pressure in the near-Earth plasma sheet greatly increases due to enhanced convection, leading to larger pressure gradients. Due to the strong stretching of the tail flux tubes, the difference $\Delta\psi$ between ψ_{out} (the flux on the outer boundary at $R \approx 18.5\, R_E$) and ψ_{in} (on the inner boundary at $R \approx 3.5\, R_E$) becomes smaller compared to quiet times. The increase in $|\partial P/\partial R|$ coupled with the decrease in $\partial\psi/\partial R$ leads to very large $|\partial P/\partial\psi|$ and thus current densities (at midnight $\alpha = \phi$ and $J_\phi = \mathbf{J} \cdot \boldsymbol{\nabla}\phi/|\boldsymbol{\nabla}\phi| = R\partial P/\partial\psi$) localized in the near-Earth plasma sheet. In our study a large gradient in the flux volume $V = \int ds/B$ is not needed in order to have large $|\partial P/\partial\psi|$, unlike in adiabatic formalisms of current sheet formation such as the "gradient of flux volume mechanism" (GFVM) [*Wiegelmann and Schindler*, 1995].

Acknowledgments This work was supported by NASA grant No. W-10062 and DoE contract No. DE-AC02-76-CH03073. S. Zaharia would like to thank Dr. Jay R. Johnson for helpful discussions. We acknowledge Dr. N. A. Tsyganenko for use of the T96 model, and D. McCune for use of the NTCC modules PSPLINE and EZcdf.

References

Becker, U., et al., On the quasistatic development of thin current sheets in magnetotail-like magnetic fields, *J. Geophys. Res.*, *106*(A3), 3811, 2001.

Birn, J., and K. Schindler, Thin current sheets in the magnetotail and the loss of equilibrium, *J. Geophys. Res.*, *107*(A7), 1117, doi: 10.1029/2001JA000291, 2002.

Birn, J., et al., Open and closed magnetospheric tail configurations and their stability, *Astrophys. and Space Sci.*, *35*, 389, 1975.

Borovsky, J. E., et al., The transport of plasma sheet material from the distant tail to geosynchronous orbit, *J. Geophys. Res.*, *103*, 20297, 1998.

Cheng, C. Z., Three-dimensional magnetospheric equilibrium with isotropic pressure, *Geophys. Res. Lett.*, *22*, 2401, 1995.

Cheng, C. Z., and A. T. Y. Lui, Kinetic ballooning instability for substorm onset and current disruption observed by AMPTE/CCE, *Geophys. Res. Lett.*, *25*(21), 4091, 1998.

De Michelis, P., et al., An average image of proton plasma pressure and of current systems in the equatorial plane derived from AMPTE/CCE-CHEM measurements, *J. Geophys. Res.*, *104*, 28615, 1999.

Iijima, T., and T. A. Potemra, The amplitude distribution of field-aligned currents at northern high latitudes observed by Triad, *J. Geophys. Res.*, *81*, 2165, 1976.

Lee, L. C., et al., Entropy antidiffusion instability and formation of a thin current sheet during geomagnetic substorms, *J. Geophys. Res.*, *103*, 29419, 1998.

Lui, A. T. Y., et al., Current disruptions in the near-Earth neutral sheet region, *J. Geophys. Res.*, *97*, 1461, 1992.

Samson, J. C., et al., Proton aurora and substorm intensifications, *Geophys. Res. Lett.*, *19*, 2167, 1992.

Sanny, J., et al., Growth-phase thinning of the near-Earth current sheet during the CDAW 6 substorm, *J. Geophys. Res.*, *99*(A4), 5805, 1994.

Sergeev, V. A., et al., Current sheet thickness in the near-earth plasma sheet during substorm growth phase, *J. Geophys. Res.*, *95*, 3819, 1990.

Spence, H. E., and M. G. Kivelson, Contributions of the low-latitude boundary layer to the finite width magnetotail convection model, *J. Geophys. Res.*, *98*, 15487, 1993.

Spence, H. E., et al., Magnetospheric plasma pressures in the midnight meridian: Observations from 2.5 to 35 R_E, *J. Geophys. Res.*, *94*, 5264, 1989.

Tsyganenko, N. A., and T. Mukai, Tail plasma sheet models derived from Geotail particle data, *J. Geophys. Res.*, *108*(A3), doi:10.1029/2002JA009707, 2003.

Tsyganenko, N. A., and D. P. Stern, Modeling the global magnetic field of the large-scale Birkeland current systems, *J. Geophys. Res.*, *101*, 27187, 1996.

Vasyliunas, V. M., Mathematical models of magnetospheric convection and its coupling to the ionosphere, in *Particles and Fields in the Magnetosphere, ed. B. M. McCormac, D. Reidel, Hingham, MA*, pp. 60–71. 1970.

Wang, C. P., et al., Modeling the inner plasma sheet protons and magnetic field under enhanced convection, *J. Geophys. Res.*, *108*(A2), 1074, doi: 10.1029/2002JA009620, 2003.

Wiegelmann, T., and K. Schindler, Formation of thin current sheets in a quasistatic magnetotail model, *Geophys. Res. Lett.*, *22*, 2057, 1995.

Wing, S., and P. T. Newell, Central plasma sheet ion properties as inferred from ionospheric observations, *J. Geophys. Res.*, *103*, 6785, 1998.

Wolf, R. A., The quasi-static (slow-flow) region of the magnetosphere, in *Solar-Terrestrial Physics*, pp. 303–368. Kluwer Academic, 1983.

Zaharia, S., et al., 3-D Force-balanced magnetospheric configurations, *submitted to Ann. Geophys.*, 2003.

This preprint was prepared with the AGU LaTeX macros v3.0. File pp˙CSpaper formatted 2003 April 2.

With the extension package 'AGU^{++}', version 1.2 from 1995/01/12

External Distribution

Plasma Research Laboratory, Australian National University, Australia
Professor I.R. Jones, Flinders University, Australia
Professor João Canalle, Instituto de Fisica DEQ/IF - UERJ, Brazil
Mr. Gerson O. Ludwig, Instituto Nacional de Pesquisas, Brazil
Dr. P.H. Sakanaka, Instituto Fisica, Brazil
The Librarian, Culham Laboratory, England
Mrs. S.A. Hutchinson, JET Library, England
Professor M.N. Bussac, Ecole Polytechnique, France
Librarian, Max-Planck-Institut für Plasmaphysik, Germany
Jolan Moldvai, Reports Library, MTA KFKI-ATKI, Hungary
Dr. P. Kaw, Institute for Plasma Research, India
Ms. P.J. Pathak, Librarian, Insitute for Plasma Research, India
Ms. Clelia De Palo, Associazione EURATOM-ENEA, Italy
Dr. G. Grosso, Instituto di Fisica del Plasma, Italy
Librarian, Naka Fusion Research Establishment, JAERI, Japan
Library, Plasma Physics Laboratory, Kyoto University, Japan
Research Information Center, National Institute for Fusion Science, Japan
Dr. O. Mitarai, Kyushu Tokai University, Japan
Dr. Jiangang Li, Institute of Plasma Physics, Chinese Academy of Sciences, People's Republic of China
Professor Yuping Huo, School of Physical Science and Technology, People's Republic of China
Library, Academia Sinica, Institute of Plasma Physics, People's Republic of China
Librarian, Institute of Physics, Chinese Academy of Sciences, People's Republic of China
Dr. S. Mirnov, TRINITI, Troitsk, Russian Federation, Russia
Dr. V.S. Strelkov, Kurchatov Institute, Russian Federation, Russia
Professor Peter Lukac, Katedra Fyziky Plazmy MFF UK, Mlynska dolina F-2, Komenskeho Univerzita, SK-842 15 Bratislava, Slovakia
Dr. G.S. Lee, Korea Basic Science Institute, South Korea
Institute for Plasma Research, University of Maryland, USA
Librarian, Fusion Energy Division, Oak Ridge National Laboratory, USA
Librarian, Institute of Fusion Studies, University of Texas, USA
Librarian, Magnetic Fusion Program, Lawrence Livermore National Laboratory, USA
Library, General Atomics, USA
Plasma Physics Group, Fusion Energy Research Program, University of California at San Diego, USA
Plasma Physics Library, Columbia University, USA
Alkesh Punjabi, Center for Fusion Research and Training, Hampton University, USA
Dr. W.M. Stacey, Fusion Research Center, Georgia Institute of Technology, USA
Dr. John Willis, U.S. Department of Energy, Office of Fusion Energy Sciences, USA
Mr. Paul H. Wright, Indianapolis, Indiana, USA

The Princeton Plasma Physics Laboratory is operated
by Princeton University under contract
with the U.S. Department of Energy.

Information Services
Princeton Plasma Physics Laboratory
P.O. Box 451
Princeton, NJ 08543

Phone: 609-243-2750
Fax: 609-243-2751
e-mail: pppl_info@pppl.gov
Internet Address: http://www.pppl.gov